Available online at www.sciencedirect.com
ScienceDirect
Aerosol Science 37 (2006) 1618–1628
Journal of Aerosol Science
www.elsevier.com/locate/jaerosci

Collection of submicron particles by an electrostatic precipitator using a dielectric barrier discharge

Jeong Hoon Byeon[a], Jungho Hwang[a,*], Jae Hong Park[a], Ki Young Yoon[a], Byung Ju Ko[a], Suk Hoon Kang[b], Jun Ho Ji[b]

[a]*Department of Mechanical Engineering, Yonsei University, Seoul 120-749, Republic of Korea*
[b]*Division of Digital Appliance Network, Samsung Electronics Co., Ltd., Suwon 442-742, Republic of Korea*

Received 1 February 2006; received in revised form 4 May 2006; accepted 8 May 2006

Abstract

Although dielectric barrier discharge (DBD) in air has been used to clean hazardous air pollutants (HAPs) because of its high electron density and energy, its potential use as precharging dust aerosol particles is not well known. In this work, we measured the size distributions of bimodal submicron aerosol particles and estimated the collection efficiency of the particles for a hybrid two-stage electrostatic precipitator (ESP) comprised of a DBD charger as the particle charger and an ESP as charged particle collector. Nano-sized particles of NaCl (30–100 nm) and DOS (50–800 nm) were generated by evaporation–condensation and atomization, respectively. Various electrical and flow conditions were applied on the DBD charger: AC applied voltage of 9–11 kV, frequency of 60–120 Hz, and air flow rate of 60–180 L min^{-1} (0.048–0.016 s of particle residence time). The particle collection efficiencies increased as the AC applied voltage increased at a fixed frequency–flow rate, whereas the efficiencies decreased as the frequency and flow rate increased at a fixed AC power–flow rate and a fixed AC applied voltage–frequency.

Keywords: Dielectric barrier discharge; Bimodal submicron aerosol particles; Collection efficiency; Two-stage electrostatic precipitator

1. Introduction

Dielectric barrier discharge (DBD) is well known to produce highly non-equilibrium plasmas in a controllable way at atmospheric pressure, and this method can effectively generate atoms, radicals, and excited species with energetic electrons at moderate gas temperatures (Abdel-Salam et al., 2003; Massines et al., 1988). The DBD usually is comprised of two electrodes that are separated by a gas gap spacing and at least one of which should be covered with dielectric material. In most DBD configurations operating at atmospheric pressure, tiny short lived current filaments, called microdischarges, are formed. The filaments contain energetic electrons (mean electron energies of typically 1–10 eV) and are separated by a typical gap spacing of 0.5 mm–1 cm. They are applied with AC voltages (typically 500 V–20 kV at 1 Hz–1 MHz) with electron densities of about 10^{14}–10^{15} cm^{-3} (Pashaie, Sankaranarayanan, & Dhali, 1999; Penetrante & Shultheis, 1993). A large fraction of the electron energy released by microdischarges can be used to dissociate gas molecules and thereby produce ions. The wide range of discharge characteristics depend on factors such as DBD

* Corresponding author. Fax: +82 2 312 2821.
E-mail address: hwangjh@yonsei.ac.kr (J. Hwang).

0021-8502/$ - see front matter © 2006 Elsevier Ltd. All rights reserved.
doi:10.1016/j.jaerosci.2006.05.003

geometry, material, type of applied voltage, and so on (Gibalov & Pietsch, 2000; Mizuno, 2000). An alternating voltage is typically used to induce microdischarges.

Until recently, DBD has been mainly used as an effective ozone generator (Eliasson, Hirth, & Kogelschatz, 1987; Gutierrez-Tapia, 1998; Samaranayake et al., 2000, 2001). Now, however, researchers are investigating the feasibility of DBD application for a wide range of fields. Since the DBD serves as a chemical reactor that produces chemical active species under various reactions, it has been used to remove certain undesired species interesting for environmental applications. An experimental study on the removal of NO_x in flue gas was carried out by Takaki, Jani, and Fujiwara (1999) and Yamamoto et al. (2004), who used plasma chemical reactions in the DBD. Breault and McLarnon (1992) used rod type electrodes and quartz tubes to study NO oxidation. Removal of SO_2 from simulated gas streams was experimentally investigated using the DBD, and also studied by computer modeling (Chang, Balbach, Rood, & Kushner, 1991). Simultaneous removal of SO_2 and NO by use of the DBD was reported by Dhali and Sardja (1991), Sun, Pashaie, Dhali, and Honea (1996), and Yamamoto, Okubo, Nagaoka, and Hayakawa (2000). Higashi, Uchida, Suzuki, and Fujii (1992) investigated the simultaneous reduction of NO_x, SO_x, and soot. Rosocha, Coogan, and Kang (1994) attempted to remove VOCs and freon gas using various types of DBD reactors. Moreover, DBD technologies were recently studied for charge neutralization of fine particles and simultaneous removal of fine particulates and gaseous contaminants. The first study on the particle charge neutralization using a DBD charger was carried out by Kwon, Sakurai, Seto, and Kim (2006). Kawada et al. (1999) and Kuroda et al. (2003) attempted to decontaminate fine carbon particles and NO_x by using a two-stage electrostatic precipitator (ESP), where the typical wire-to-plate charging section was replaced by a DBD charger. Although it is known that fine particulates smaller than 10 μm and gaseous pollutants can be controlled effectively with the barrier discharge type ESP, these are very few published results for the collection of submicron particles.

In this study, we experimentally investigated the collection characteristics of submicron aerosol particles by using a lab-scale, two-stage, and barrier discharge type ESP. First the particles were charged in the DBD charger. Then the charged particles were collected in the ESP. Test aerosol of bimodal size distribution was generated with an electrically heated tube furnace (20–100 nm, NaCl) and an atomizer (50–800 nm, dioctyl sebacate (DOS)). While the voltage, frequency, and flow rate in the DBD charger were varied, the number concentration of particles that penetrated through the ESP was measured with a scanning mobility particle sizer (SMPS) system.

2. Experimental

The schematic diagram of our experimental setup is shown in Fig. 1. The experimental setup consists of a test particle supply section, power supply–detection section, test duct section, and particle detection section. Particle-free compressed air from a dry clean air supply system was distributed to both an electrically heated tube furnace (Lenton Furnaces, Model GTF 12/25/364) and a Collision type atomizer. The remaining air was supplied to a diluter to dilute NaCl particles generated from the tube furnace (path A) and also to dilute the mixture of NaCl and DOS (density $= 0.915\,\mathrm{g\,cm^{-3}}$) particles (generated from the atomizer) and thus control the flow rate through the test duct (path B).

Sodium chloride (NaCl) particles were stably generated from the electrically heated tube furnace at 700 °C. The length and the inner diameter of the ceramic tube were 364 and 25.4 mm, respectively. The air flow rate supplied to the ceramic tube was maintained at $3\,\mathrm{L\,min^{-1}}$. The generated NaCl particles were mixed and diluted with dry clean air of $15\,\mathrm{L\,min^{-1}}$ in the diluter ⓐ. The DOS particles were generated from the atomizer of a solution containing DOS (20 vol%) mixed with isopropyl alcohol (80 vol%). The desired concentrations of NaCl and DOS particles were controlled, respectively, with two laminar flow meters. Fig. 2 shows the size distributions of NaCl and DOS particles. The size ranges of NaCl and DOS particles were 20–100 and 50–800 nm, respectively. Details of the size distributions are summarized in Table 1. NaCl and DOS particles were mixed in a mixing tube, and the mixture showed a bimodal size distribution, as shown in Fig. 2.

The mixture of test particles was again diluted with dry clean air in the diluter ⓑ. The dilution ratio was controlled within the range of 1–200. The inlet flow rate (or particle residence time) to the duct was varied to 60 (0.048 s), 120 (0.032 s), and $180\,\mathrm{L\,min^{-1}}$ (0.016 s) by adjusting the rotameter, which was calibrated by a digital mass flow meter (TSI 3302). After the test aerosol entered the test duct (cross-sectional area of $80 \times 20\,\mathrm{mm^2}$), it was electrically charged in the DBD charger and then supposed to be subsequently collected in the ESP. As shown in Fig. 3, the DBD charger

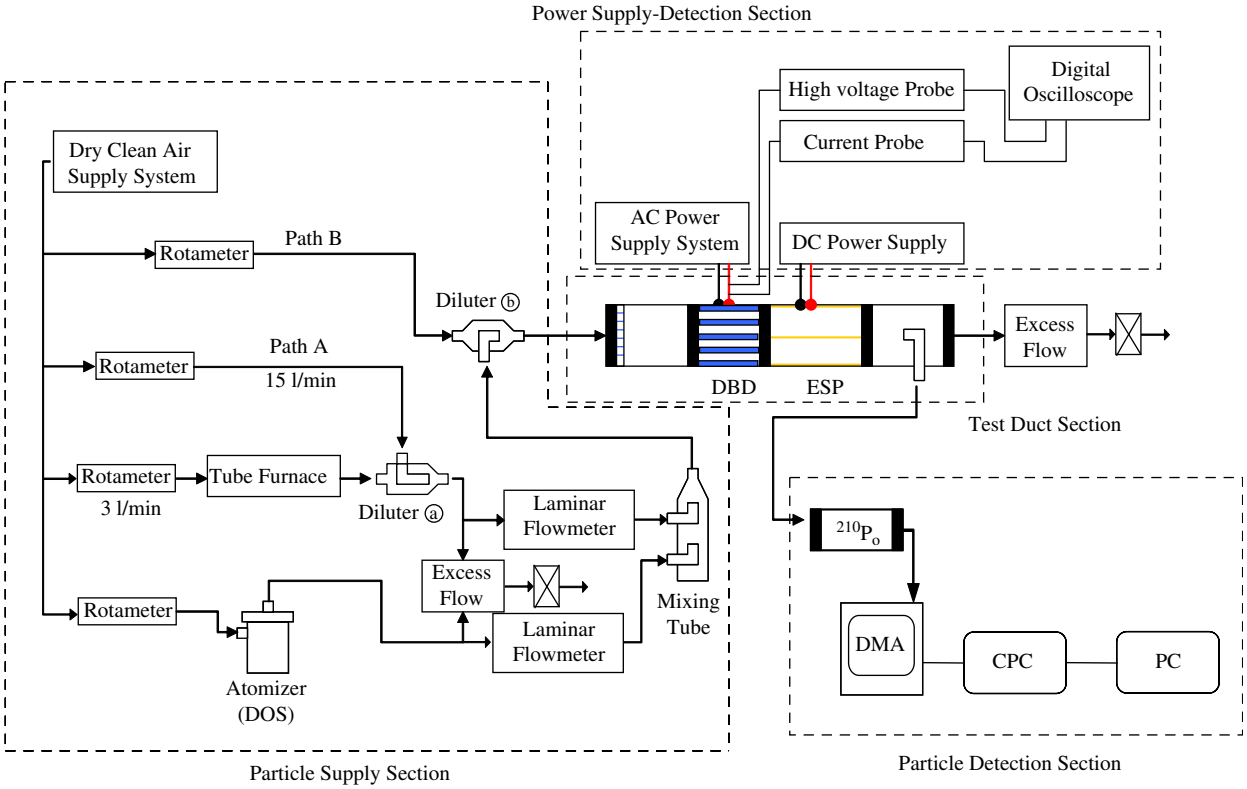

Fig. 1. Schematics of experimental setup.

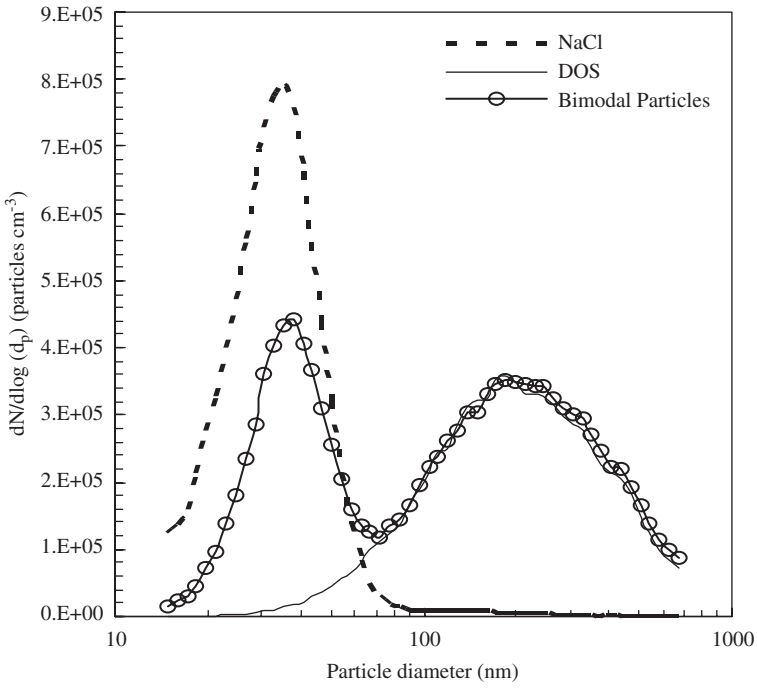

Fig. 2. Particle size distributions.

Table 1
Characteristics of particle size distributions

Test aerosol	NaCl	DOS
Geometric mean diameter (nm)	31	213
Geometric standard deviation	1.47	1.88
Concentration (# cm^{-3})	8×10^5	3.5×10^5

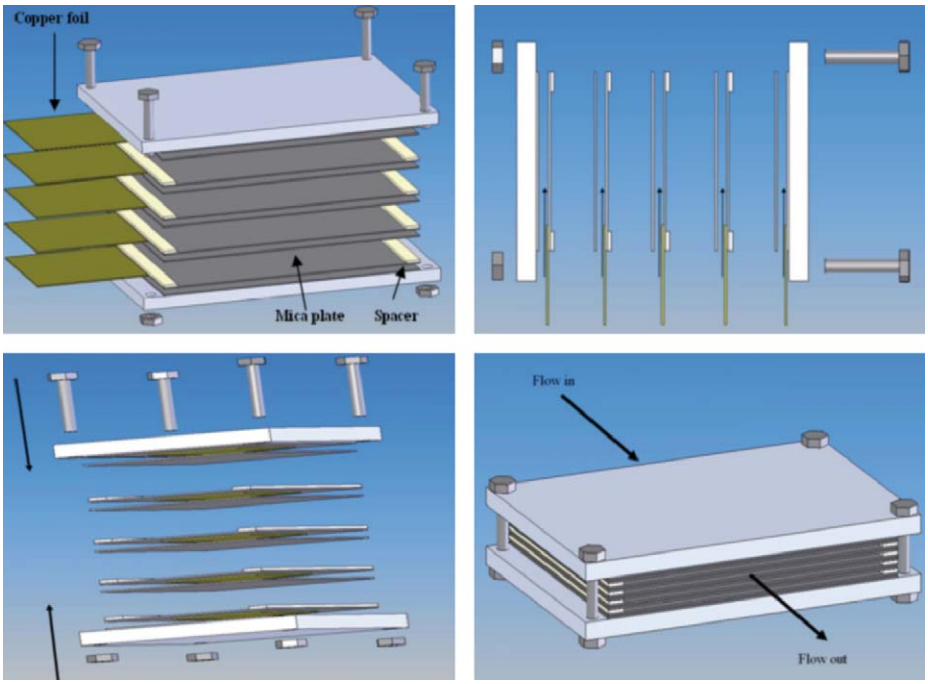

Fig. 3. Detailed geometries of DBD charger.

consisted of five parallel plate electrodes, three of which were grounded. A high sinusoidal AC voltage was applied to the other two electrodes. The gap spacing between a grounded electrode and its adjacent powered electrode was 4 mm. Each electrode was made of 0.03 mm thick copper foil (30 mm of streamwise length and 80 mm of spanwise length) sandwiched between two 0.3 mm thick dielectric plates (mica plates, 40 mm of streamwise length and 100 mm of spanwise length). The ESP consisted of three parallel copper plate electrodes (200 mm of streamwise length and 80 mm of spanwise length), two of which were grounded. A high negative DC voltage (−8 kV) was applied to the other electrode (cathode) located in the center. The spacing between the grounded electrode and the cathode was 10 mm.

An SMPS (TSI 3936), composed of a differential mobility analyzer (TSI 3081) and a condensation particle counter (CPC, TSI 3022A), was used as the particle measurement system. An aerosol charge neutralizer containing radioactive source ^{210}Po was adopted in this study. The structure of the ^{210}Po aerosol charge neutralizer is similar to that of the ^{85}Kr aerosol charge neutralizer (TSI 3077). Flow rates of the sampling and the sheath of the SMPS system were 0.3 and 3.0 L min^{-1}, respectively.

The fractional (grade) collection efficiency of the DBD charger (η_{DBD}), excluding diffusional wall loss and, thus, including only electrostatic deposition, is defined by

$$\eta_{DBD}(d_p) = 1 - \frac{C_D(d_p)}{C_0(d_p)}. \quad (1)$$

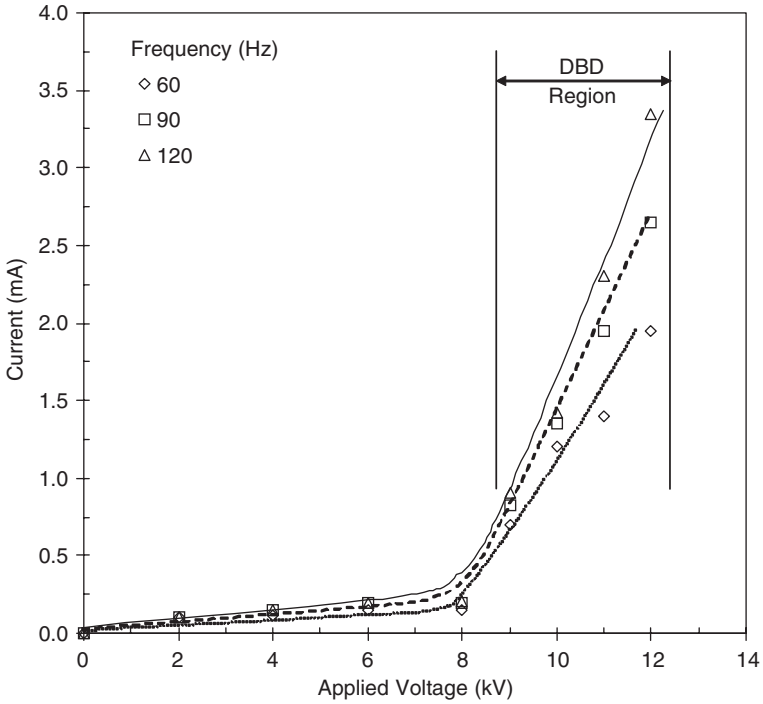

Fig. 4. I–V characteristics of DBD charger.

$C_0(d_p)$ is the concentration of particle size d_p measured at the exit of the ESP when the powers applied to both the DBD charger and the ESP were turned off. The particle size is the mobility equivalent diameter. $C_D(d_p)$ is the concentration when only the power to the DBD charger is on (without the ESP energization). Since new particles might be generated in the DBD charger when the power to the DBD was on, experiments were carried out. When no test aerosol particles were injected to the DBD charger, the maximum concentration of generated particles was less than $20\,\#\,cm^{-3}$. Similarly, the fractional collection efficiency of the ESP (η_{ESP}) due to only electrostatic deposition is defined by

$$\eta_{ESP}(d_p) = 1 - \frac{C_E(d_p)}{C_D(d_p)}. \tag{2}$$

$C_E(d_p)$ is the concentration when both the DBD charger and the ESP were on (with the ESP energization). The fractional total collection efficiency (η_{Total}) can be expressed as

$$\eta_{Total}(d_p) = 1 - (1 - \eta_{DBD})(1 - \eta_{ESP}) = 1 - \frac{C_E(d_p)}{C_0(d_p)}. \tag{3}$$

Fig. 4 shows voltage–current characteristics for the frequency range of 60–120 Hz. DBD voltage and current were measured by a four-channel digital oscilloscope (LeCroy 9302M). Their root-mean-square (RMS) amplitude values are indicated in Fig. 4. For the frequency range, the stable DBD was maintained at applied voltages of 8–12 kV, but the transition to arc occurred at voltages higher than approximately 13 kV. Higher frequency resulted in higher discharge current. The discharge currents were 0.7–1.4, 0.82–1.95, and 0.91–2.3 mA for frequencies of 60, 90, and 120 Hz, respectively. Fig. 5 shows voltage and current profiles as a function of time when the RMS voltage and frequency were 9 kV and 60 Hz, respectively.

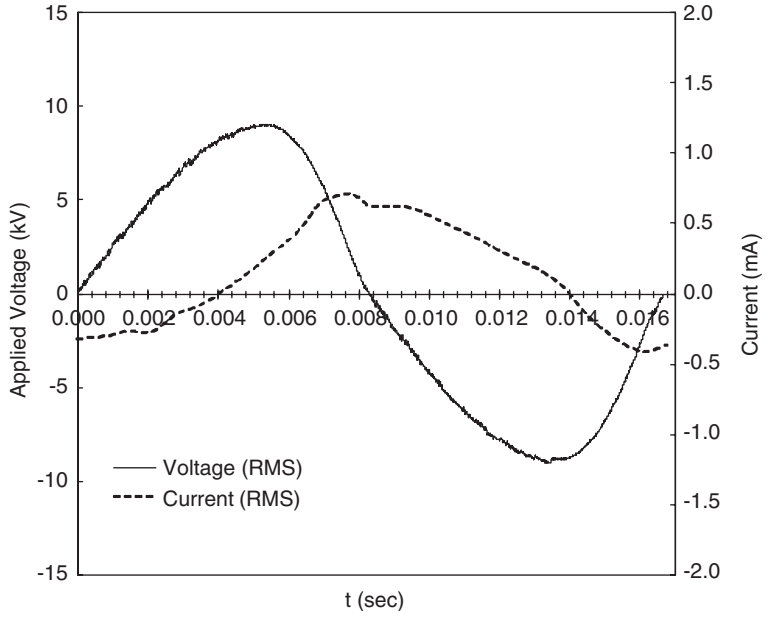

Fig. 5. Typical voltage and current profiles (at 9 kV, 60 Hz).

3. Results and discussion

Experiments were carried out to obtain collection efficiencies, η_{DBD} and η_{Total}, for various electrical conditions of AC voltage–frequency and air flow rates. First, the particle size distribution was measured while both powers to the DBD charger and to the ESP were off. Then, the particle size distributions were measured when the AC voltage and frequency applied to the DBD charger were varied as 9–11 kV and 60–120 Hz, respectively, but the DC power to the ESP was off. Next, the variation of particle size distributions was investigated when the DC voltage of −8 kV was additionally supplied to the ESP.

Particle collection efficiencies, η_{DBD}, are plotted in Fig. 6 as a function of the particle diameter for voltage–current levels of 9–0.7, 10–1.2, and 11 kV–1.4 mA. The results were obtained at frequency of 60 Hz and air flow rate of 60 L min^{-1}. The results imply that the AC power applied to the DBD charger charged the aerosol particles, which were, thereafter, precipitated on the DBD charger.

Preliminary experiments were carried out to evaluate the particle charge distributions with two methods: fluorometric method and tandem differential mobility analyzer (TDMA) method. The particles were bipolarly charged but the number of positively charged particles was much higher than that of negatively charged particles. We think that because the positive and negative charge carriers are different in electrical mobility and mass, the quick drift of negative charge carriers (maybe electrons) toward the wall of the DBD charger occurred, and, consequently, the positive charging ratio was substantially higher than the negative charging ratio (asymmetric charging) after the DBD charger. Further study on measurements of charge distribution after the DBD charger is under way.

For any voltage–current level, the electrostatic efficiency of the DBD charger can be expressed as the following equation by assuming well-mixed flow caused by turbulence:

$$\eta_{\mathrm{DBD}}(d_{\mathrm{p}}) = 1 - \exp[-kEZ], \tag{4}$$

where E is the intensity of the applied electric field and k is a constant depending on the flow characteristics. Z is the electrical mobility which is expressed as

$$Z \sim \frac{n(d_{\mathrm{p}})C(d_{\mathrm{p}})}{d_{\mathrm{p}}}. \tag{5}$$

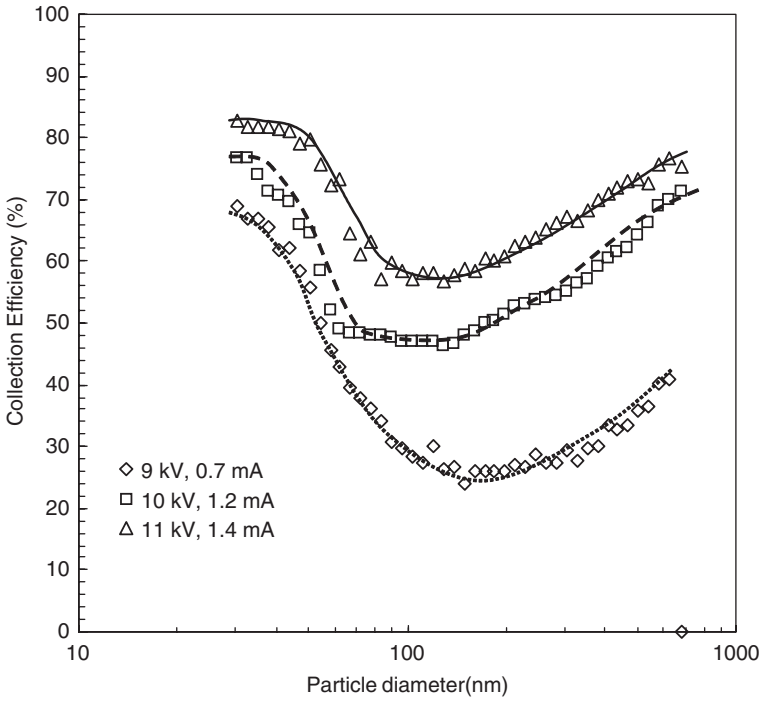

Fig. 6. η_{DBD} with AC power (DBD on and ESP off, at 60 Hz, 60 L min^{-1}).

$C(d_p)$ is the Cunningham correction factor, which depends on d_p and can be approximated as $3.69(\lambda/d_p)^{1/2}$ (λ: mean free path of air molecules) for the intermediate range of λ/d_p (Lee & Liu, 1980). $n(d_p)$ is the average number of elementary charges of a particle, which depends on the particle size and charging characteristics. Even in the presence of electrostatic fields, diffusion charging is the predominant mechanism for charging particles less than 200 nm in diameter. For these small particles, $n(d_p)$ is proportional to $d_p \ln(1 + \alpha d_p)$, where α is the constant related to ion–particle collisions. For particles larger than about 200 nm in diameter, field charging is the dominant mechanism and $n(d_p) \sim d_p^2$ (Cardello, Volckens, Tolocka, Wiener, & Buckley, 2002; Huang & Chen, 2001; Mizuno, 2000). Therefore, for $d_p < \sim 200$ nm, Z is proportional to $d_p^{-1/2}$ and thus η_{DBD} decreases as d_p increases, while for $d_p > \sim 200$ nm, Z is proportional to $d_p^{1/2}$ and thus η_{DBD} increases as d_p increases. This theoretical prediction of η_{DBD} well agreed with experimental data shown in Fig. 6. The higher the AC applied voltage, the higher the collection efficiencies for all sizes of particles because of the higher particle charging in the DBD charger.

Even though the particles escaped from the DBD charger, they were collected additionally at the ESP when DC voltage (−8 kV) was applied to the ESP. The fractional collection efficiencies of the ESP (η_{ESP}), due to only electrostatic deposition, are shown in Fig. 7 for three voltage–current levels. The results show that η_{ESP} increased as d_p increased for the entire size range. Especially, the efficiency of particles of 100–200 nm in diameter substantially increased to 70–85%, even though these particles were highly penetrable from the DBD charger. After combining the results in Figs. 6 and 7 with Eq. (3), the total fractional efficiencies could be summarized, as shown in Fig. 8. The results in Fig. 8 show that the staged precipitation with the DBD charger and the ESP substantially enhanced the efficiencies, especially for particles less than about 200 nm in diameter.

Fig. 9. shows the effect of AC frequency (60–120 Hz) on η_{DBD} for constant discharge power (15.4 W) and flow rate (60 L min^{-1}). The results show that the collection efficiency decreased as the frequency increased. In the AC DBD charger the gas-entrained particles were subject to both a field and charging ions of alternating polarity as discussed by Ehrlich and Melcher (1987). The time for ions to migrate across the DBD charger electrode, τ, is approximately expressed as $H/\mu E$, where H is the electrode spacing, μ is the electrical mobility of the ions, and E is the electrical field. Since $E \approx \rho H/\varepsilon_0$ (ρ: space charge density, ε_0: permittivity of free space) is derived from Gauss Law $\nabla \cdot E = \rho/\varepsilon_0$, the characteristic time for positive and negative ions is $\tau_\pm = \varepsilon_0/\rho_\pm\mu_\pm$. The subscript $\pm$ refers to positive and negative ions,

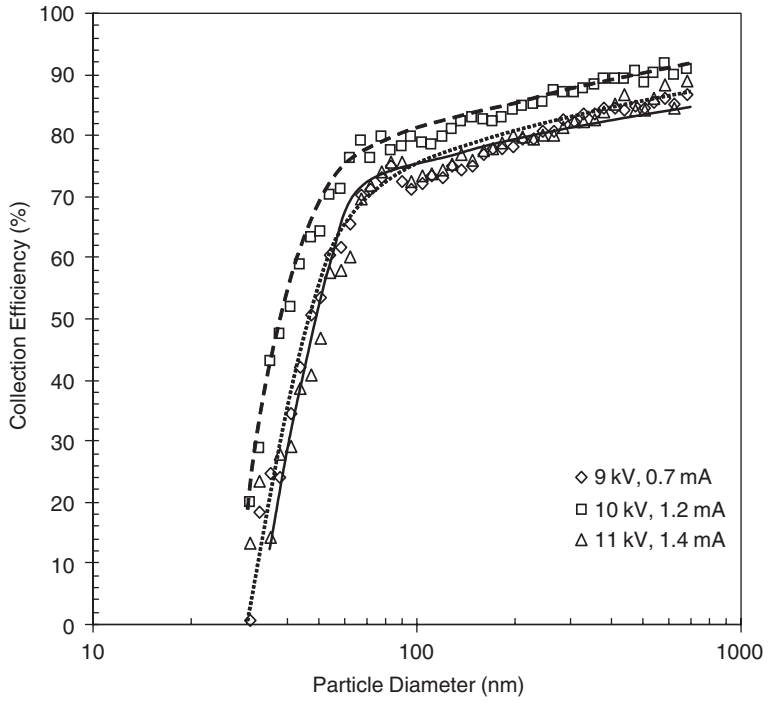

Fig. 7. η_{ESP} with AC power (DBD on and ESP on, at 60 Hz, 60 L min^{-1}).

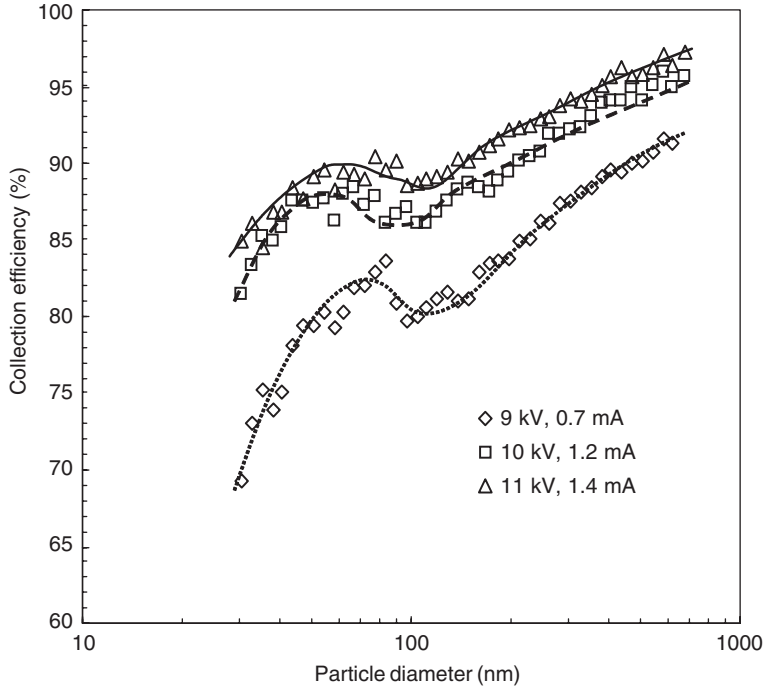

Fig. 8. η_{Total} with AC power (DBD on and ESP on, at 60 Hz, 60 L min^{-1}).

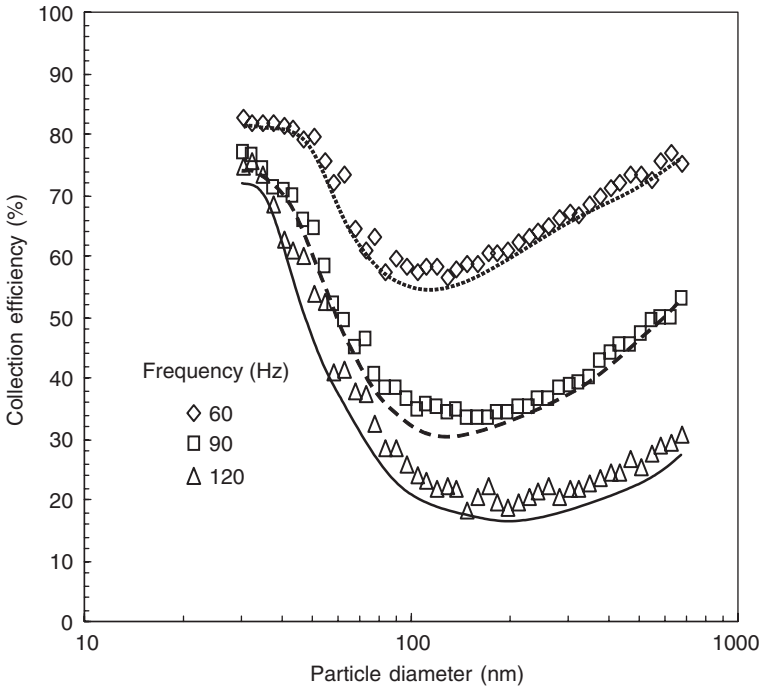

Fig. 9. η_{DBD} with frequency (at 15.4 W, 60 L min^{-1}).

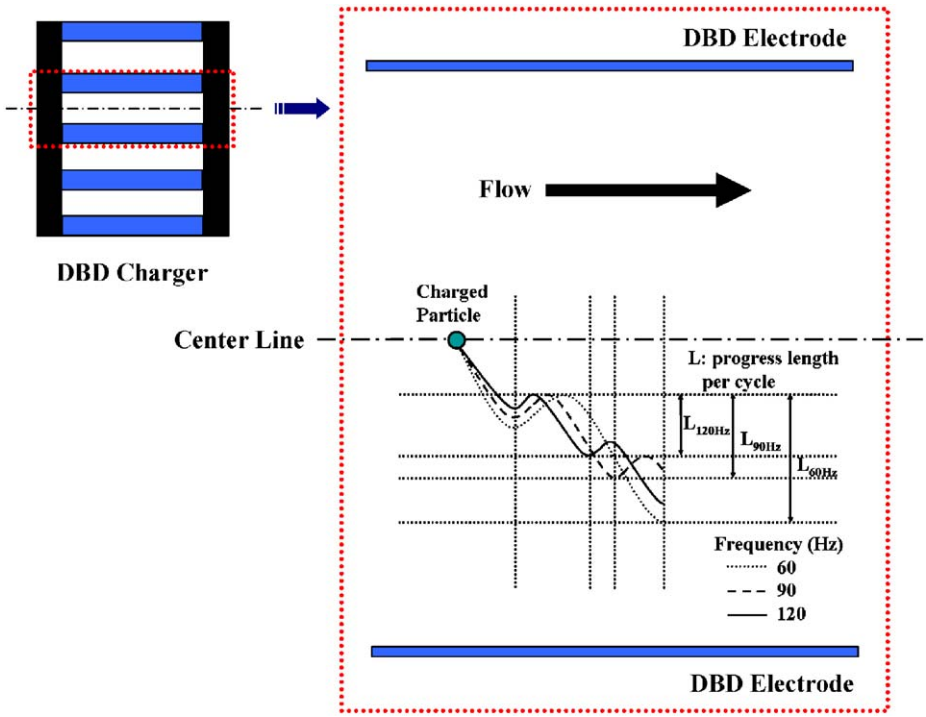

Fig. 10. Particle trajectory in DBD charger.

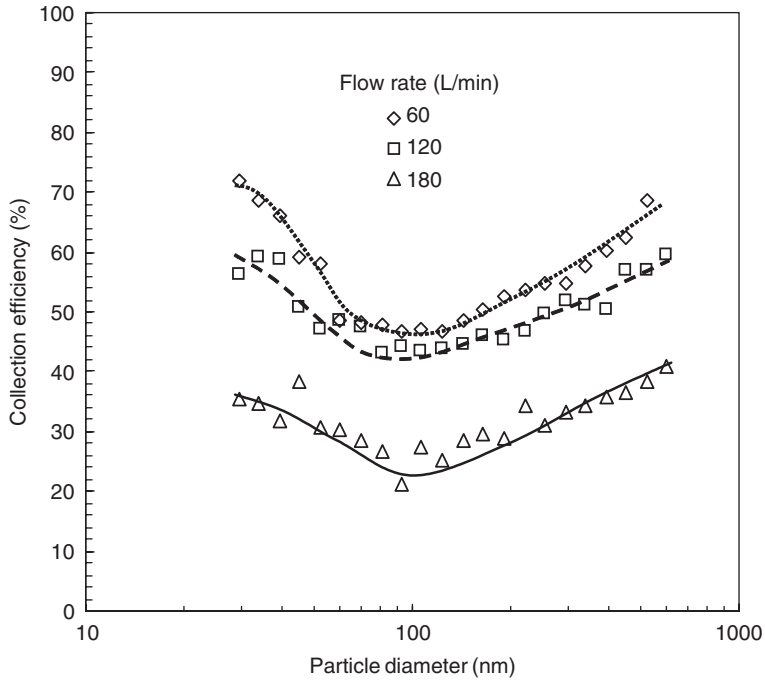

Fig. 11. η_{DBD} with flow rate (at 10 kV, 60 Hz).

respectively. If the period of excitation T, which is inversely proportional to the frequency, is long compared to τ, the field and charge variations are in phase. Thus, in a flow directed from left to right with a vertically directed alternating field and the source of particles at the top, a charged particle has a trajectory like that shown in Fig. 10.

The particle initially moves downward but changes direction because a part of each half-cycle is spent discharging the particle. The amount of time that the particle spends during each half-cycle with a charge of the same sign as that of the ions around it, relative to the time it spends with an opposite charge, is determined by the ratio of the cycle time T to the characteristic time $\tau_{\pm}$. Certainly, if the cycle time T is longer than the characteristic time, then particles reverse their charge shortly after the field reverses. In this case, they will spend most of each half-cycle migrating toward an electrode. From an opposite view, the particles spend a significant fraction of each half-cycle with ions, neutralizing the charge that existed at the end of the previous half-cycle and hence migrating in the wrong direction, making little net progress toward the DBD charger electrode.

The effect of flow rate of the DBD charger on the collection efficiency is discussed with Fig. 11. The flow rate of the DBD charger was varied from 60 to 180 L min^{-1} so that the residence time of the particles could be approximately from 0.048 to 0.016 s. The higher the flow rate (or shorter residence time), the lower the collection efficiencies for all sizes of particles because of the less chances of ion–particle collisions in the DBD charger.

4. Conclusions

We measured the size distributions of bimodal submicron aerosol particles and estimated the collection efficiency of the particles for a hybrid two-stage electrostatic precipitator (ESP) comprised of a DBD charger as the particle charger and an ESP as the charged particle collector. Various electrical and flow conditions were applied on the DBD charger: AC applied voltage of 9–11 kV, frequency of 60–120 Hz, and air flow rate of 60–180 L min^{-1} (0.048–0.016 s of particle residence time). The particle collection efficiencies increased as AC applied voltage increased at a fixed frequency–flow rate, whereas the efficiencies decreased as the frequency and flow rate increased at a fixed AC power–flow rate and a fixed AC applied voltage–frequency.

Further investigations will follow about the different electrical parameters of the DBD charger to obtain more information on the submicron-sized particle collection characteristics.

Acknowledgment

This work was supported by the Korean Science and Engineering Foundation (KOSEF) project for "Fundamentally Specified Research Project" under Grant R01-2005-000-10723-0.

References

Abdel-Salam, M., Hashem, A., Yehia, A., Mizuno, A., Turky, A., & Gabr, A. (2003). Characteristics of corona and silent discharges as influenced by geometry of the discharge reactor. *Journal of Physics D*, *36*, 252–260.

Breault, R. W., & McLarnon, M. (1992). Reaction kinetics for flue gas treatment of NO_x. *Proceedings of NATO advanced research workshop on non-thermal plasma techniques for pollution control* (pp. 239–256), Cambridge, England.

Cardello, N., Volckens, J., Tolocka, M. P., Wiener, R., & Buckley, J. (2002). Performance of a personal electrostatic precipitator particle sampler. *Aerosol Science and Technology*, *36*, 162–165.

Chang, M. B., Balbach, J. H., Rood, M. J., & Kushner, M. J. (1991). Removal of SO_2 from gas streams using a dielectric barrier discharge and combined plasma photolysis. *Journal of Applied Physics*, *69*(8), 4409–4417.

Dhali, S. K., & Sardja, I. (1991). Dielectric-barrier discharge for processing of SO_2/NO_x. *Journal of Applied Physics*, *69*(9), 6319–6324.

Ehrlich, R. M., & Melcher, J. R. (1987). AC corona charging of particles. *IEEE Transactions on Industry Applications*, *IA-23*(1), 103–107.

Eliasson, B., Hirth, M., & Kogelschatz, U. (1987). Ozone synthesis from oxygen in dielectric barrier discharges. *Journal of Physics D*, *20*, 1421–1437.

Gibalov, V. I., & Pietsch, G. J. (2000). The development of dielectric barrier discharges in gas gaps and on surfaces. *Journal of Physics D*, *33*, 2618–2636.

Gutierrez-Tapia, C. (1998). Dynamics of ozone generation in a silent oxygen discharge. *IEEE Transactions on Plasma Science*, *26*(4), 1357–1362.

Higashi, M., Uchida, S., Suzuki, N., & Fujii, K. (1992). Soot elimination and NO_x and SO_x reduction in diesel-engine exhaust by a combination of discharge plasma and oil dynamics. *IEEE Transactions on Plasma Science*, *20*(1), 1–12.

Huang, S. H., & Chen, C. C. (2001). Filtration characteristics of a miniature electrostatic precipitator. *Aerosol Science and Technology*, *35*, 792–804.

Kawada, Y., Kubo, T., Ehara, Y., Ito, T., Zukeran, A., Takahashi, T., Kawakami, H., & Takamatsu, T. (1999). Development of high collection efficiency ESP by barrier discharge system. *Industry applications conference IEEE* (Vol. 2, pp. 1130–1135).

Kuroda, Y., Kawada, Y., Takahashi, T., Ehara, Y., Ito, T., Zukeran, A., Kono, Y., & Yasumoto, K. (2003). Effect of electrode shape on discharge current and performance with barrier discharge type electrostatic precipitator. *Journal of Electrostatics*, *57*, 407–415.

Kwon, S. B., Sakurai, H., Seto, T., & Kim, Y. J. (2006). Charge neutralization of submicron aerosols using surface-discharge microplasma. *Journal of Aerosol Science*, *37*, 483–499.

Lee, K. W., & Liu, B. Y. H. (1980). On the minimum efficiency and the most penetrating particle size for fibrous filters. *Journal of the Air Pollution Control Association*, *30*, 377–381.

Massines, F., Rabehi, A., Decomps, P., Gadri, R. B., Ségur, P., & Mayoux, C. (1988). Experimental and theoretical study of a glow discharge at atmospheric pressure controlled by dielectric barrier. *Journal of Applied Physics*, *83*, 2950–2957.

Mizuno, A. (2000). Electrostatic precipitation. *IEEE Transactions on Dielectrics and Electrical Insulation*, *7*(5), 615–624.

Pashaie, B., Sankaranarayanan, R., & Dhali, S. K. (1999). Experimental investigation of microdischarges in a dielectric-barrier discharge. *IEEE Transactions on Plasma Science*, *27*(1), 22–23.

Penetrante, B. M., & Shultheis, E. S. (1993). *Non-thermal plasma techniques for pollution control*. Berlin, Heidelberg, Germany: Springer.

Rosocha, L. A., Coogan, J. J., & Kang, M. (1994). Use of silent electrical discharges for environmental remediation. *IEEE international conference* (p. 88).

Samaranayake, W. J. M., Miyahara, Y., Namihira, T., Katsuki, S., Hackam, R., & Akiyama, H. (2000). Ozone production using pulsed dielectric barrier discharge in oxygen. *IEEE Transactions on Dielectrics and Electrical Insulation*, *7*(6), 849–854.

Samaranayake, W. J. M., Miyahara, Y., Namihira, T., Katsuki, S., Hackam, R., & Akiyama, H. (2001). Ozone generation in dry air using pulsed discharges with and without a solid dielectric layer. *IEEE Transactions on Dielectrics and Electrical Insulation*, *8*(4), 687–697.

Sun, W., Pashaie, B., Dhali, S. K., & Honea, F. I. (1996). Non-thermal plasma remediation of SO_2/NO using a dielectric-barrier discharge. *Journal of Applied Physics*, *79*(7), 3438–3444.

Takaki, K., Jani, M. A., & Fujiwara, T. (1999). Removal of nitric oxide in flue gases by multipoint to plane dielectric barrier discharge. *IEEE Transactions on Plasma Science*, *27*(4), 1137–1145.

Yamamoto, K., Yukimura, M., Kambara, S., Moritomi, H., Yamashita, T., & Maruyama, T. (2004). Effect of O_2 on NO removal by ammonia radical injection using one-cycle sinusoidal power source. *Thin Solid Films*, *457*, 39–43.

Yamamoto, T., Okubo, M., Nagaoka, T., & Hayakawa, K. (2000). Simultaneous removal of NO_x and SO_x in flue gas emission using plasma-chemical hybrid process. *Industry applications conference IEEE* (Vol. 1, pp. 641–647).